Noble-gas quenching of rovibrationally excited H_2

N. Balakrishnan*,† and Bradley C. Hubartt
Department of Chemistry, University of Nevada-Las Vegas, Las Vegas, Nevada 89154, USA

Luke Ohlinger and Robert C. Forrey*,‡
Department of Physics, Penn State University, Berks Campus, Reading, Pennsylvania 19610-6009, USA
(Received 20 April 2009; published 10 July 2009)

Collisions between noble-gas atoms and hydrogen molecules are investigated theoretically by solving the time-independent Schrödinger equation. Various initial states of the molecule are considered and the calculations are performed for each system over a large range of collision energies. Cross sections for quenching of rovibrationally excited states of H_2 are reported for Ar and Kr colliders and comparisons are made with previous calculations involving He. For both Ar and Kr colliders, the effect of vibrational excitation is found to be more pronounced for ortho-H_2. The $T \rightarrow 0$ limit of the total quenching rate coefficient, which is presented here as the imaginary part of a complex scattering length, is found to increase by about 7 orders of magnitude as the vibrational quantum number of ortho-H_2 is increased from 1 to 10. Trends in the energy dependence for the heavier systems are very similar, including resonance behavior, which suggest that the dynamics of heavy noble-gas H_2 systems are less sensitive to the fine details of the potential.

DOI: 10.1103/PhysRevA.80.012704 PACS number(s): 34.50.Ez

I. INTRODUCTION

Buffer gas cooling is a proven technique for cooling atoms and molecules and loading them into magnetic traps [1]. These experiments typically use a cryogenic cell filled with ^{3}He buffer gas to cool the desired atoms or molecules via elastic collisions. Inelastic collisions generally play a destructive role in the cooling process due to an unwanted release of energy. Motivated by such experiments, dynamical studies have been performed for a variety of ultracold He collision systems including the molecules CaH [2], NH [3], YbF [4], CO [5–7], and O_2 [8,9] which have an electric or magnetic dipole moment. Experimental confirmation of many ultracold collision predictions have yet to be realized; but with the rapid advancement of the field of ultracold molecular physics [10,11], we may expect an increasingly wider range of collision systems and processes to be studied. The first studies of ultracold molecule collisions with helium were for H_2 [12]. Follow-up studies for this system [13–15] have provided the most exhaustive and reliable set of theoretical cross sections for an atom-diatom collision. These calculations have revealed interesting behavior for the collisional dynamics of H_2 in highly excited rovibrational states. For example, quasiresonant vibration rotation (QRVR) energy transfer was found to occur for some highly rotationally excited states at ultracold temperatures [13]. Because many other excited states do not undergo QRVR transitions, very sharp structures were found in the rotational distributions of the cross sections [16,17]. Similar behavior was observed for Ar+H_2 in the ultracold limit [18]. The energy dependence for this system, however, revealed the existence of shape resonances [19] that were not seen in the case of He. Later calculations for He+H_2 showed an emergence of the shape resonances for many of the rotationally excited states near dissociation [15]. Therefore, it seems that the resonance behavior for H_2 collisions has a strong dependence on the anisotropy of the potential-energy surface (PES). In order to gain a better understanding of this dependence, we extend the H_2 studies to include additional calculations for He and Ar colliders and to include Kr+H_2 where a reliable potential is readily available [20]. The *ab initio* He [21] potential has been shown [12] to accurately reproduce measured values [22] of vibrational relaxation rate coefficients. The binding energy of the He-H_2 van der Waals complex predicted [12] using this potential was found to be in close agreement with both experiment [23] and competing theory [24–26]. Likewise, the semiempirical Ar [27] and Kr [20] potentials accurately reproduce high-resolution IR spectroscopic data and are expected to be reliable. Together these three noble-gas systems represent a family whose dynamics may be quantitatively understood. This in turn should allow qualitative predictions to be made that may be useful for understanding trends in the dynamical behavior for other systems involving H_2.

II. THEORY

Generally, quenching collisions are controlled by a competition between the energy and angular momentum gaps between the initial and final internal states of the system. For a light diatom such as H_2, the rotational energy-level spacings are large enough that rovibrational transitions are able to provide relatively small energy gaps without severely increasing the angular momentum gaps. The large internal energy spacings also allow a close-coupling formulation to achieve numerical convergence to within a few percent using basis sets of modest size. The basis states for the close-coupling calculations are constructed from numerical solutions to the diatomic Schrödinger equation

*Corresponding author.
†naduvala@unlv.nevada.edu
‡rcf6@psu.edu

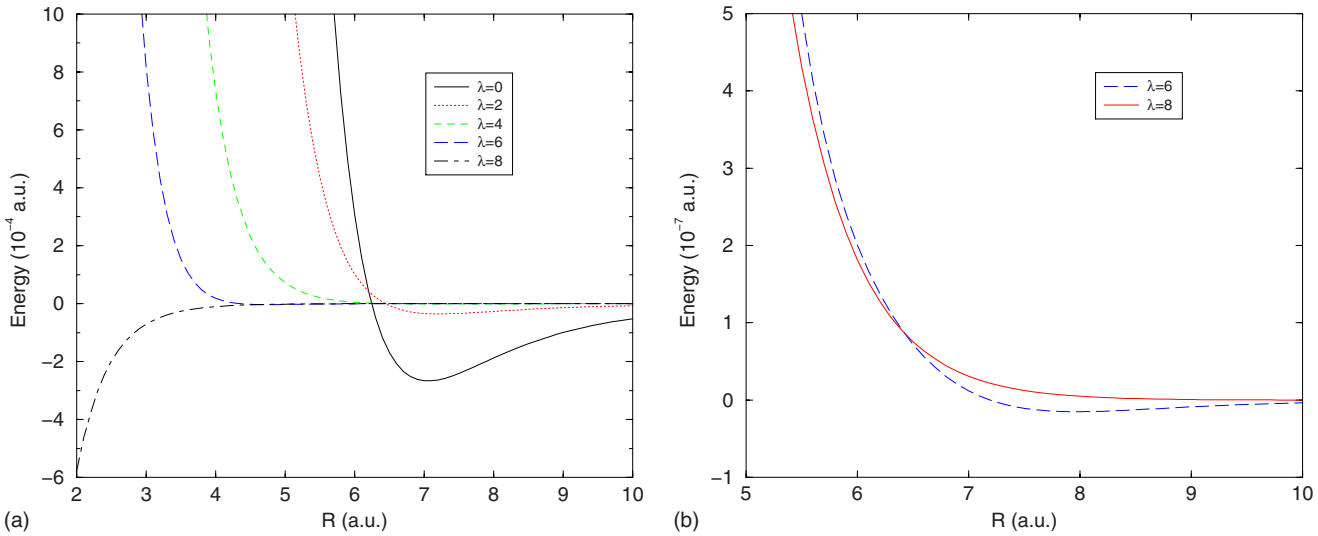

FIG. 1. (Color online) Potential-energy matrix elements for Kr+H_2. The diagonal elements $v^{\lambda}_{10\to 10}$ are shown in the left panel and the off-diagonal elements $v^{6}_{10\to 06}$ and $v^{8}_{10\to 08}$ in the right panel.

$$\left[\frac{1}{2m}\frac{d^2}{dr^2} - \frac{j(j+1)}{2mr^2} - v(r) + \epsilon_{vj}\right]\chi_{vj}(r) = 0, \tag{1}$$

where m and $v(r)$ are the reduced mass and potential of H_2, and v and j are the vibrational and rotational quantum numbers for the eigenstate χ_{vj}. The eigenvalues ϵ_{vj}, which are the rovibrational energy levels of the H_2 molecule, are obtained by diagonalization in a basis set of Laguerre or Hermite polynomials. The coupled channel Schrödinger equation is solved using the MOLSCAT program of Hutson and Green [28]. The state-to-state cross sections are given by

$$\sigma_{vj\to v'j'} = \frac{\pi}{2\mu E_{vj}(2j+1)}\sum_{J=0}^{\infty}(2J+1)\sum_{l=|J-j|}^{|J+j|}\sum_{l'=|J-j'|}^{|J+j'|}|\delta_{jj'}\delta_{ll'}\delta_{vv'} - S^{J}_{vjl;v'j'l'}|^2, \tag{2}$$

where μ is the atom-diatom reduced mass, E_{vj} is the translational energy for the initial state, $S^{J}_{vjl;v'j'l'}$ is a scattering matrix element, and J and l are the total angular momentum and orbital angular momentum quantum numbers, respectively.

It is convenient, both for computational purposes and analysis, to expand the interaction potential in terms of Legendre polynomials

$$V_l(\vec{r},\vec{R}) = \sum_{\lambda}^{\infty} v_{\lambda}(r,R)P_{\lambda}(\cos\,\theta). \tag{3}$$

The reduced potential coupling matrix elements required for the scattering calculation may be obtained from

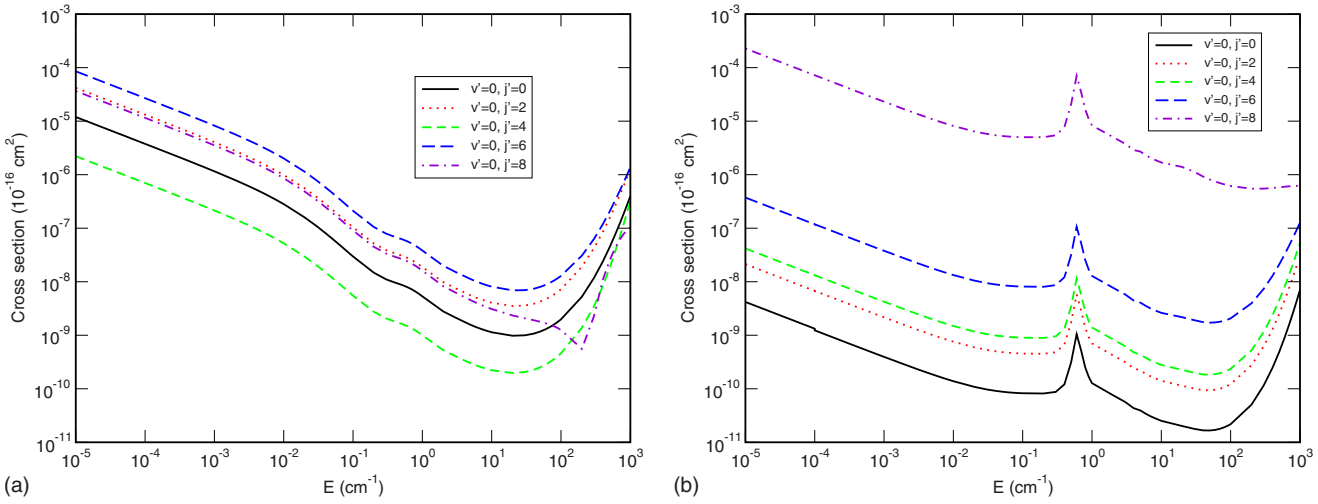

FIG. 2. (Color online) State-to-state cross sections for para-H_2 collisions with helium (left panel) and krypton (right panel). The initial and final molecular states are $(v=1, j=0)$ and (v', j'), respectively. The overall shapes and relative strengths of the cross sections for Kr are similar to those for Ar [19].

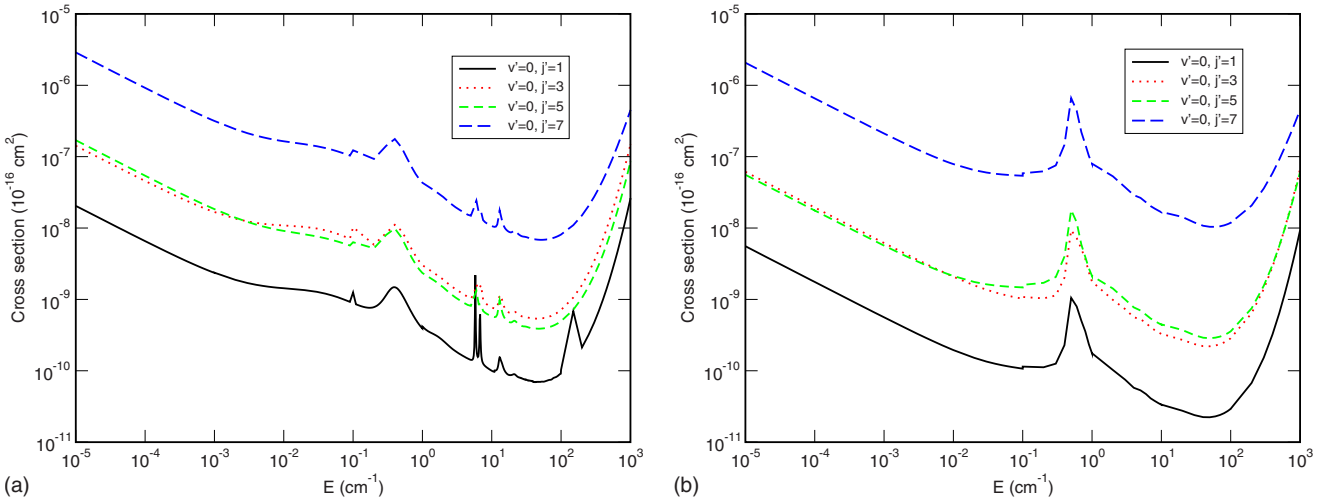

FIG. 3. (Color online) State-to-state cross sections for ortho-H_2 collisions with argon (left panel) and krypton (right panel). The initial and final molecular states are $(v=1,j=1)$ and (v',j'), respectively.

$$v^{\lambda}_{vj\to v'j'}(R) = \int_0^{\infty} \chi^{*}_{vj}(r) v_{\lambda}(r,R) \chi_{v'j'}(r) dr. \tag{4}$$

Insight into the efficiency of inelastic transitions may be gained by comparing off-diagonal couplings to the repulsive barrier of the incoming channel. Figure 1 shows such a comparison for $Kr+H_2(v=1,j=0)$. The left panel of the figure shows that at low collision energies, the classical turning point in the $v=1,j=0$ channel is located around 6 a.u. Therefore, any off-diagonal coupling that occurs at distances less than 6 a.u. will not play a significant role in the scattering process. The right panel of the figure shows the off-diagonal matrix elements $v^{6}_{10\to 06}$ and $v^{8}_{10\to 08}$. These matrix elements are of comparable magnitude above the classical turning point, so we expect that the $(v=1,j=0)\to(v'=0,j'=8)$ transition will be more efficient than the $(v=1,j=0)\to(v'=0,j'=6)$ transition due to the smaller energy gap. This expectation is confirmed in the next section where cross sections for these and other transitions are given.

It is noteworthy, however, that the relative strength of these two particular transitions has been found to depend dramatically on the choice of PES for both He and Ar collision partners [14,19]. For example, the $(v=1,j=0)\to(v'=0,j'=8)$ transition for $He+H_2$ collisions was shown to be the dominant transition over a wide range of energies when the cross sections are computed using the PES of Boothroyd *et al.* [29]. This produces total quenching rate coefficients that are 1000 times larger than those obtained using the PES of Muchnick and Russek [21]. A similar situation, although less dramatic, was found for the case of $Ar+H_2$. The PES of Schwenke *et al.* [30] yielded cross sections that were dominated by the $(v=1,j=0)\to(v'=0,j'=6)$ transition, whereas cross sections computed using the PES of Bissonnette *et al.* [27] were found to be dominated by the $(v=1,j=0)\to(v'=0,j'=8)$ transition. Experiments have been used to establish the reliability of a given PES for these systems. The quenching rate coefficients obtained using the

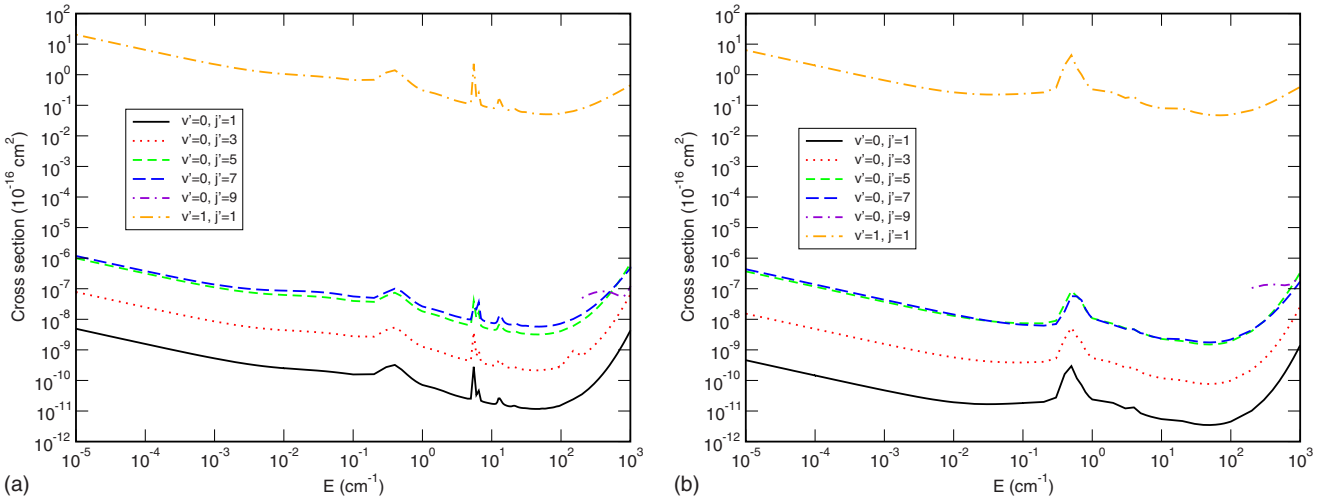

FIG. 4. (Color online) State-to-state cross sections for ortho-H_2 collisions with argon (left panel) and krypton (right panel). The initial and final molecular states are $(v=1,j=3)$ and (v',j'), respectively.

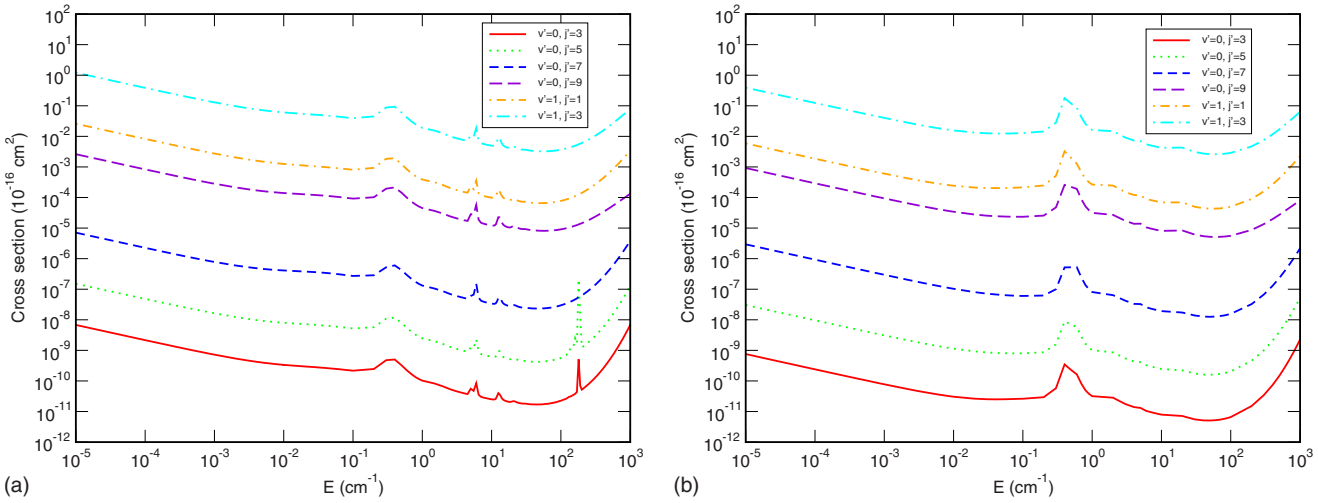

FIG. 5. (Color online) State-to-state cross sections for ortho-H_2 collisions with argon (left panel) and krypton (right panel). The initial and final molecular states are $(v=1,j=5)$ and (v',j'), respectively.

He+H_2 PES of Muchnick and Russek [21] are in close agreement with the experimental data of Audibert *et al.* [22]. The Kr+H_2 PES of Wei *et al.* [20] and the Ar+H_2 PES of Bissonnette *et al.* [27] have been shown to accurately reproduce high-resolution IR and virial coefficients data. Unless otherwise stated, the results given in the next section were computed using these potentials for He, Ar, and Kr collisions with H_2.

III. RESULTS

Figure 2 shows state-to-state cross sections for the quenching of $H_2(v=1,j=0)$ due to collisions with He and Kr. It is clear that there are substantial differences in the quenching behavior for these two noble-gas colliders. For helium, the absence of high-order anisotropic terms in the angular expansion of the interaction potential [21] favors small Δj. However, there is a complicated interplay between energy-gap and angular momentum gap behavior as may be seen by the $j'=4$ curve (which represents the weakest transition) and the $j'=6$ curve (which represents the strongest transition). The $j'=8$ curve is comparable to the $j'=2$ curve at very low collision energies but then deviates in shape from the other curves near 100 cm^{-1}. Collisions with krypton are clearly determined by energy-gap considerations as may be seen by the well-ordered curves which increase with increasing j' or, equivalently, with decreasing energy gap. It is noteworthy that the Kr results appear very similar to results previously published for Ar [19] when the PES of Bissonnette *et al.* [27] is used. Both systems show a shape resonance near 0.5 cm^{-1} that is due to the $l=2$ partial wave. The overall shapes and relative strengths of the state-to-state cross sections for Ar and Kr collisions with $H_2(v=1,j=0)$ are also similar. Unlike the He case, the anisotropy of the interaction potential for Ar and Kr is sufficient to drive transitions to $j'=8$ with very high efficiency. This rotational level is the highest level accessible in the $v'=0$ manifold at translational energies below 300 cm^{-1} and has the smallest energy gap

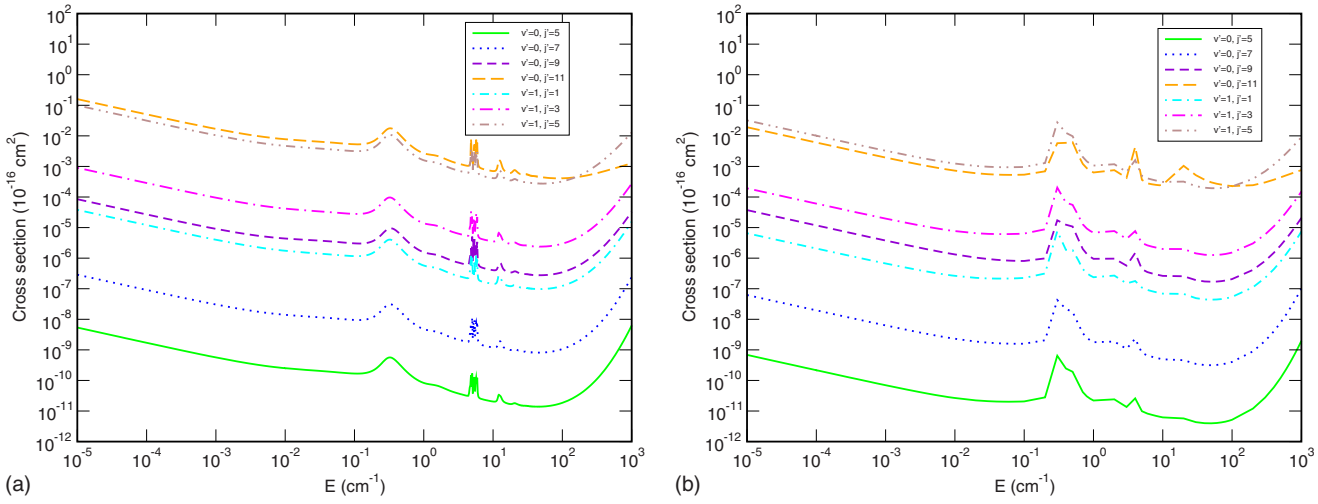

FIG. 6. (Color online) State-to-state cross sections for ortho-H_2 collisions with argon (left panel) and krypton (right panel). The initial and final molecular states are $(v=1,j=7)$ and (v',j'), respectively.

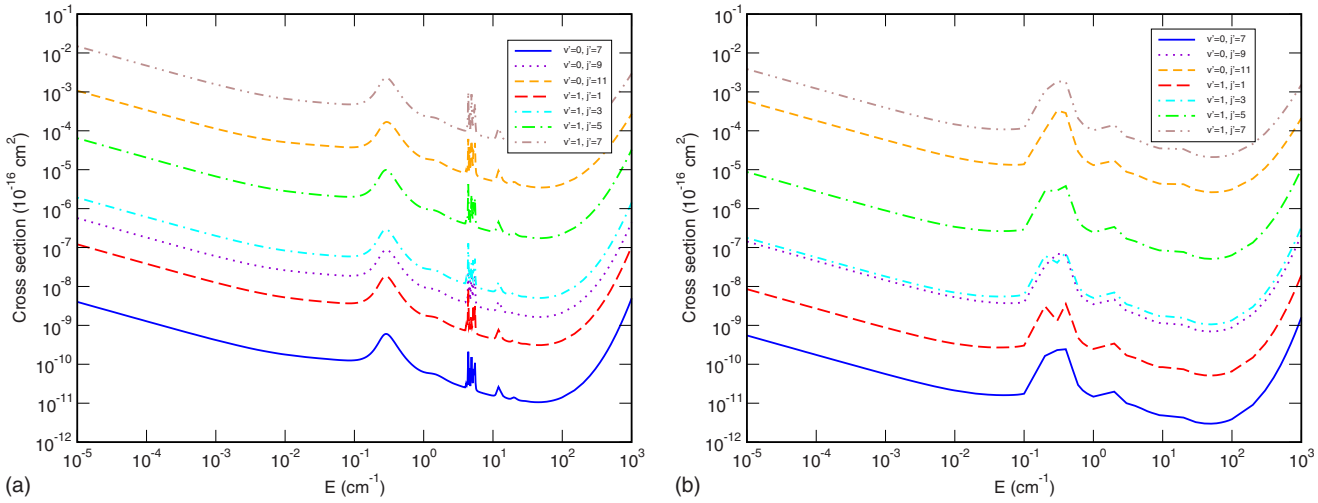

FIG. 7. (Color online) State-to-state cross sections for ortho-H_2 collisions with argon (left panel) and krypton (right panel). The initial and final molecular states are $(v=1,j=9)$ and (v',j'), respectively.

from the initial state. Because the ratio of $v^8_{10\to08}$ to $v^6_{10\to06}$ at distances beyond the classical turning point is larger for Kr $+H_2$ than for Ar$+H_2$ (compare Fig. 1 of the present work with Fig. 5 of [19]), the ratio of $j'=8$ to $j'=6$ cross sections is also larger at low collision energies ($\sim$500 for Kr versus $\sim$20 for Ar at $E=10^{-5}$ a.u.). It is also interesting to note that the minima of the quenching cross sections occur at about 10 cm^{-1} for the He-H_2 system compared to about 60–70 cm^{-1} for the Kr system. These values are comparable to the well depth of the van der Waals interaction potential for these systems. Similar behavior has been observed for rovibrational transitions in other van der Waals systems [2,5–9] and it appears to be a characteristic feature of quenching cross sections at low temperatures.

The similarity in Ar and Kr cross sections is even greater for the ortho-H_2 collisions shown in Figs. 3–7. This is due to the energetic closing of the $\Delta j=8$ transition that dominates the quenching of $H_2(v=1,j=0)$. Figure 3 shows cross sections for the $H_2(v=1,j=1)$ initial state. The $j'=7$ level is now the highest rotational level accessible at low collision energies. While the Ar results show several sharp resonances that are missing in the Kr results, a prominent shape resonance is found for both systems just below 1 cm^{-1}. The $\Delta j=6$ transition has the smallest allowable energy gap and is the dominant transition for both Ar and Kr colliders. In both cases, the $j'=1$ curve is weakest due to the large energy gap which results from pure vibrational quenching. The increasing angular momentum gap in going from $\Delta j=2$ to $\Delta j=4$ is balanced by a decreasing energy gap so that the $j'=3$ and $j'=5$ curves are nearly the same.

This trend continues for states with higher initial angular momentum. Figure 4 shows cross sections for the H_2 $(v=1,j=3)$ initial state. Again, the increasing change in internal angular momentum in going from $\Delta j=2$ to $\Delta j=4$ is balanced for $\Delta v=-1$ by a decreasing change in internal energy which produces nearly identical results for the $j'=5$ and $j'=7$ curves of both systems. These are the dominant rovibrational transitions for low collision energies due to the in-

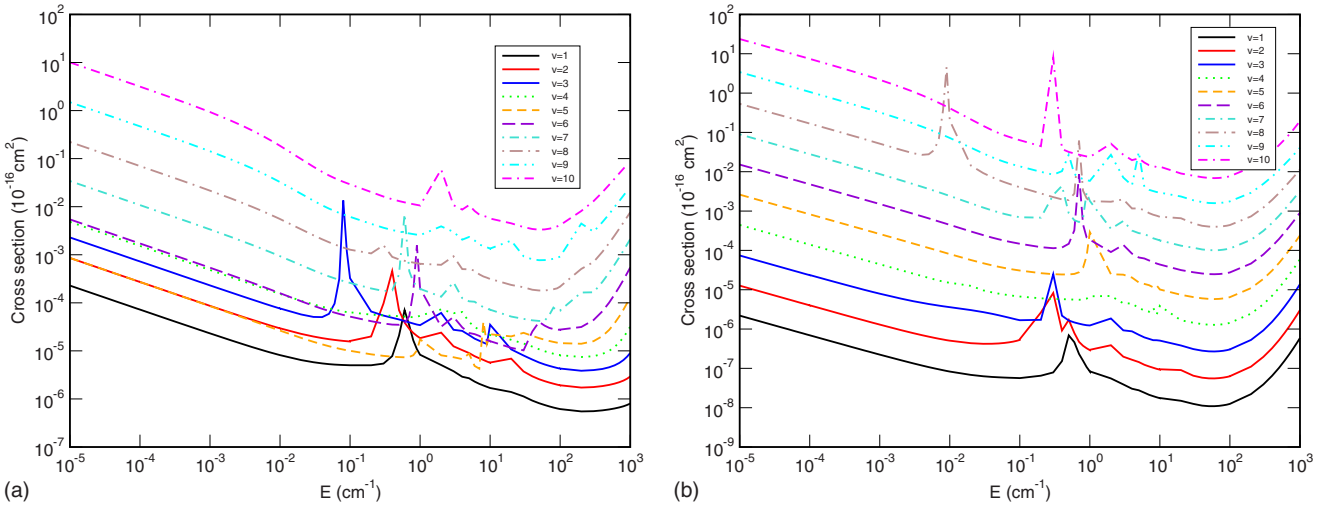

FIG. 8. (Color online) Total quenching cross sections for collisions of Kr with para-$H_2(v,j=0)$ in the left panel and ortho-$H_2(v,j=1)$ in the right panel. The curves are defined by the initial v-level shown in the legend.

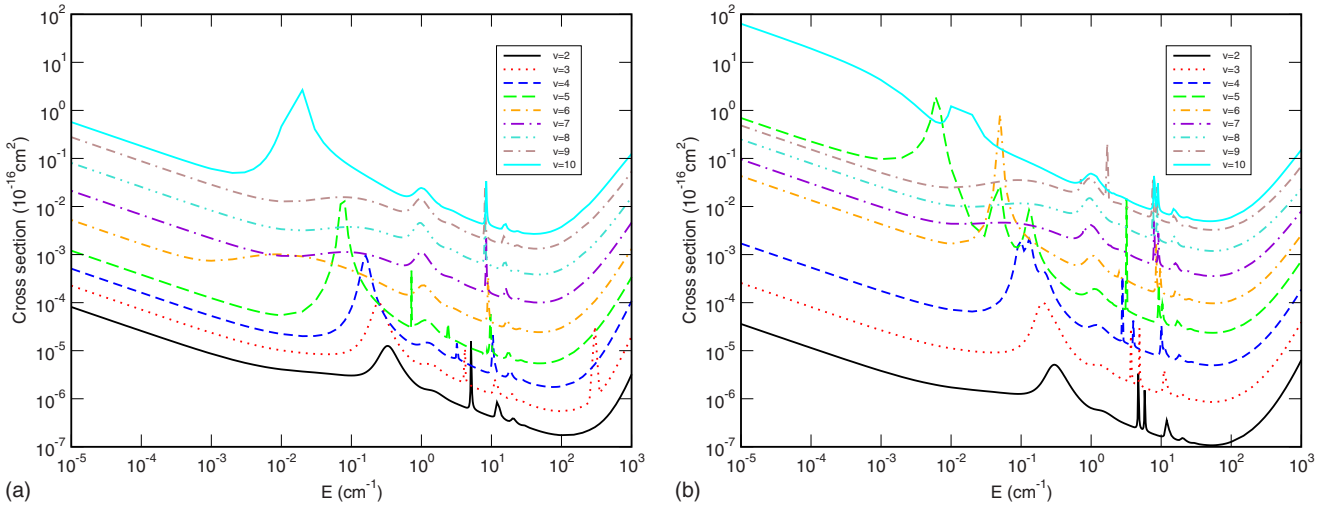

FIG. 9. (Color online) Total quenching cross sections for collisions of Ar with para-$H_2(v,j=0)$ in the left panel and ortho-$H_2(v,j=1)$ in the right panel. The curves are defined by the initial v level shown in the legend.

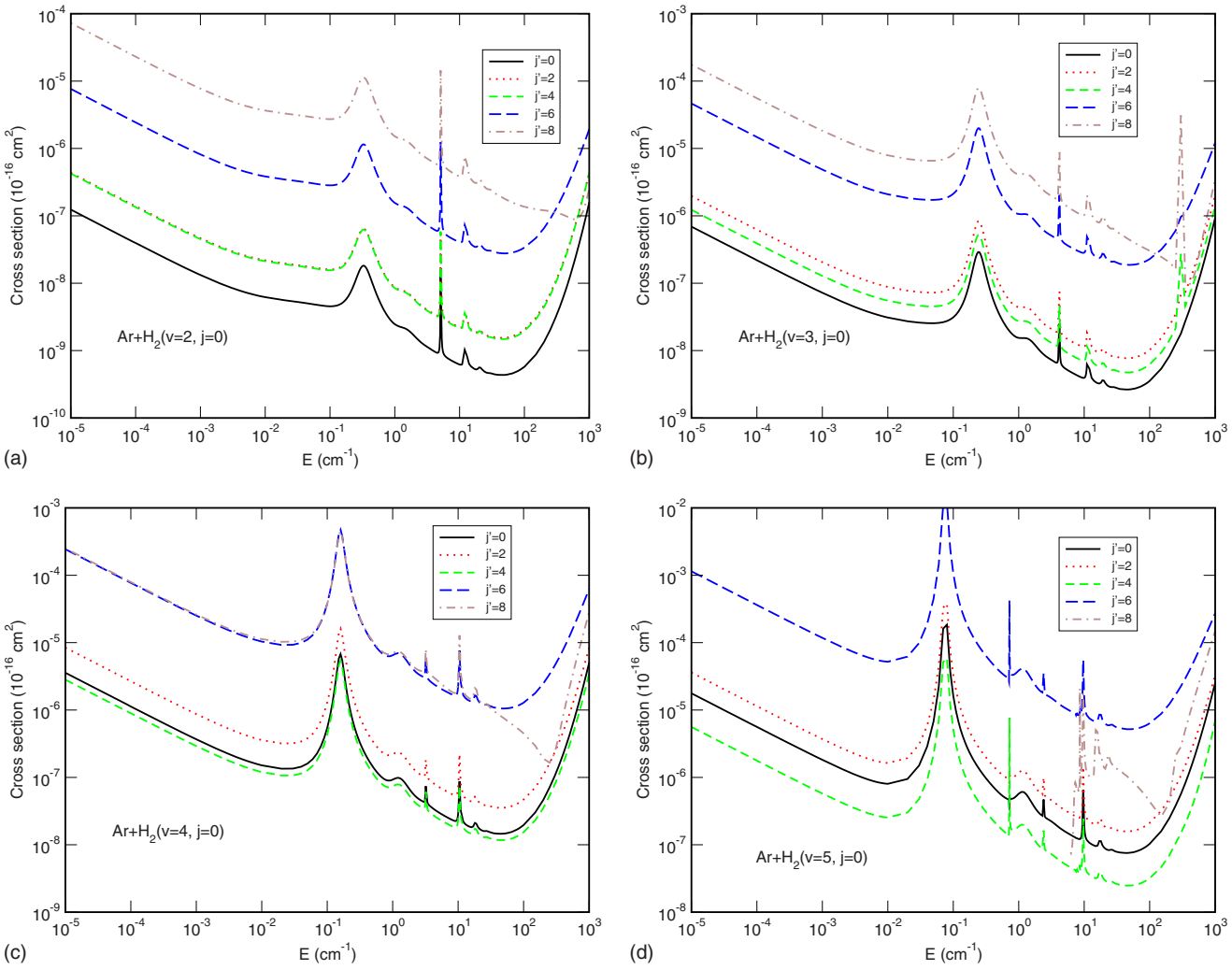

FIG. 10. (Color online) State-to-state collision cross sections for $Ar+H_2(v,j=0)$ making transitions to $H_2(v'=v-1,j')$. The curves are defined by the final rotational level shown in the legend.

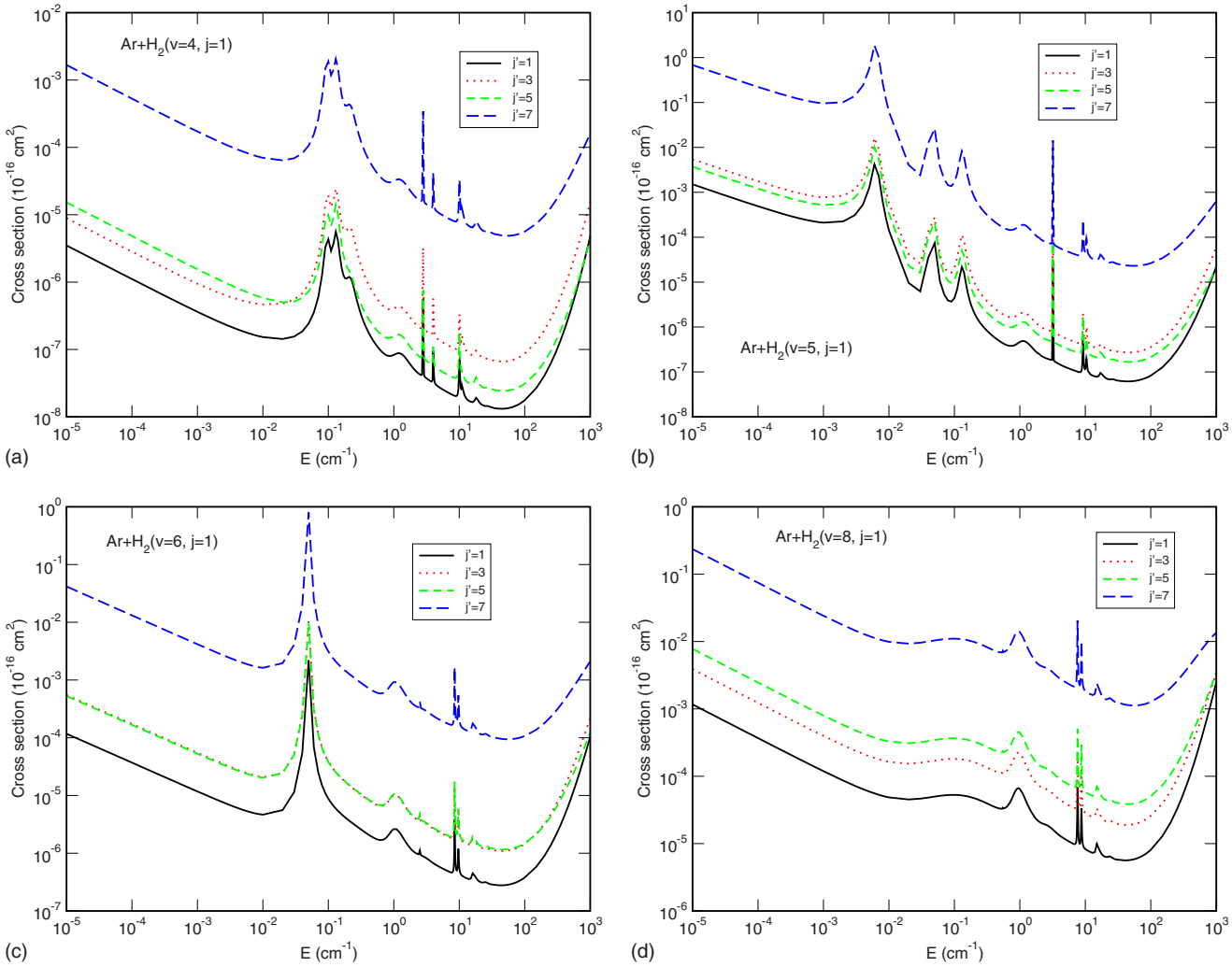

FIG. 11. (Color online) State-to-state collision cross sections for $Ar+H_2(v,j=1)$ making transitions to $H_2(v'=v-1,j')$. The curves are defined by the final rotational level shown in the legend.

accessibility of the $\Delta j=6$ transition for energies below 200 cm^{-1}. Due to the strong dependence of the interaction potential on the orientation angle compared to the stretching of the H_2 molecule, the cross sections for pure rotational quenching are found to dominate rovibrational quenching by many orders of magnitude. Similar to Fig. 3, the Ar cross sections show several sharp resonances at energies near 10 cm^{-1}, and both Ar and Kr show a prominent shape resonance below 1 cm^{-1} which is due to the $l=2$ partial wave.

Figures 5–7 show cross sections for Ar and Kr collisions with ortho-H_2 in an initial state with $v=1$ and $j=5-9$. The sets of curves for both systems continue to appear very similar to each other. The curves for rovibrational transitions with $\Delta j=2$ and $\Delta j=4$ are no longer approximately equal in magnitude; the $\Delta j=4$ transition now dominates at low energies by more than 100 times for $j=5$ and continues to separate from the $\Delta j=2$ curve as j is increased. The pure rotational transitions again dominate the quenching for $j=5$ with $\Delta j=-2$ and $\Delta j=-4$ transitions both showing larger values than the rovibrational transitions. Interestingly, this is not the case for $j=7$. The rovibrational $\Delta j=4$ transition has completely overtaken the pure rotational $\Delta j=-4$ transition and is comparable to the pure rotational $\Delta j=-2$ transition at energies below 100 cm^{-1}. This behavior is due to a QRVR energy transfer process [13]. For $j=9$, the QRVR $\Delta j=-4\Delta v$ transition is energetically closed, and the pure rotational $\Delta j=-2$ transition is again dominant.

Vibrational relaxation for states with large initial vibrational excitation has been studied for $He+H_2$ [12]. It was found that the total quenching cross-section curves for $j=0$ are well ordered with increasing magnitude as v increases all the way to the dissociation limit. Figure 8 shows that this pattern is not followed for $Kr+H_2$ due to the efficiency of the rovibrational $\Delta j=8$ transition for $v=1-4$. This transition completely dominates the $\Delta j=6$ transition (see Fig. 2) which is the next strongest contribution to the quenching. For $v>4$, the $\Delta j=8$ transition is energetically closed for collision energies below 1 cm^{-1} and the $\Delta j=6$ transition becomes the strongest. This disrupts the pattern of increasing cross sections for the quenching of $H_2(v,j=0)$ as v is increased beyond 4 units of vibration. The pattern for $v>5$ returns to a well-ordered increase in the total quenching cross section with increasing initial vibration when the collision energy is below 10^{-2} cm^{-1}. At higher energies, there is some conges-

TABLE I. Scattering lengths in angstroms.

	Ar+$H_2(j=0)$		Kr+$H_2(j=0)$		Ar+$H_2(j=1)$		Kr+$H_2(j=1)$	
v	α	β	α	β	α	β	α	β
0	9.950	0	5.678	0	9.820	0	5.842	0
1	9.088	1.628×10^{-9}	4.950	1.962×10^{-8}	8.933	2.733×10^{-10}	4.950	1.887×10^{-10}
2	8.389	6.884×10^{-9}	3.914	7.363×10^{-8}	8.199	3.053×10^{-9}	3.998	1.089×10^{-9}
3	7.809	1.915×10^{-8}	2.887	1.971×10^{-7}	7.559	2.174×10^{-8}	2.951	6.370×10^{-9}
4	7.324	4.319×10^{-8}	1.699	4.149×10^{-7}	6.926	1.442×10^{-7}	1.741	3.806×10^{-8}
5	6.927	1.022×10^{-7}	0.268	7.373×10^{-8}	2.592	5.866×10^{-5}	0.279	2.248×10^{-7}
6	6.622	4.434×10^{-7}	1.522	4.673×10^{-7}	6.784	3.640×10^{-6}	1.566	1.308×10^{-6}
7	6.432	1.801×10^{-6}	3.848	2.937×10^{-6}	6.424	8.106×10^{-6}	3.996	7.649×10^{-6}
8	6.402	6.845×10^{-6}	6.963	1.911×10^{-5}	6.357	2.111×10^{-5}	7.323	4.579×10^{-5}
9	6.589	2.350×10^{-5}	11.138	1.282×10^{-4}	6.602	4.111×10^{-5}	11.942	2.929×10^{-4}
10	6.945	4.847×10^{-5}	16.194	8.642×10^{-4}	9.419	5.408×10^{-3}	17.879	2.039×10^{-3}

tion in the curves due to the threshold behavior of the $\Delta v=-1,\Delta j=8$ transition and also the appearance of shape resonances.

The right panel of Fig. 8 shows cross sections for Kr $+H_2(v,j=1)$ as a function of energy. Because the $\Delta v=-1,\Delta j=8$ transition is not allowed at low energies for $j>0$, the total quenching cross section curves are well ordered with increasing magnitude as v is increased all the way to the dissociation limit. For both sets of curves in Fig. 8, the shape resonances tend to shift downward in energy as v is increased before disappearing. A notable exception is the resonance seen in the $v=8$ curve for ortho-H_2. This resonance occurs at an energy near 10^{-2} cm^{-1} which is roughly ten times lower than the collision energy of any other resonance. Figure 8 also reveals that, in the ultracold limit, the effect of vibrational excitation is more pronounced for the ortho-H_2 system. The cross section increases by about 7 orders of magnitude between $v=1$ and $v=10$ for the ortho case while the enhancement is only about 5 orders of magnitude for the para case.

Figure 9 shows total quenching cross sections for collisions of Ar with vibrationally excited H_2. The effect of vibrational excitation is again more pronounced for the ortho-H_2 collisions. The cross sections for Ar and Kr show comparable enhancement as v is increased. Interestingly, the para-H_2 curves are well ordered with increasing v at low energies whereas the ortho-H_2 curves are not. This is opposite to the case of Kr as seen in Fig. 8. The situation may be explained by examination of the state-to-state cross sections, which are shown in Figs. 10 and 11. For para-$H_2(v,j=0)$, the efficiency of the $\Delta j=6$ transition becomes comparable to that of the $\Delta j=8$ transition when $v=4$. Therefore, when the $\Delta j=8$ transition becomes energetically closed for $v>4$ there is no sudden drop in the total quenching cross section like there was in the case of Kr. For ortho-$H_2(v,j=1)$, the break in the ordering of the total quenching curves with increasing v is not due to a relative change in the efficiencies of rotational transitions. Instead, each of the state-to-state cross sections for $v=5$ is significantly enhanced compared to those of the neighboring vibrational levels (see Fig. 11). Such enhancement can occur when the van der Waals interaction potential supports a quasibound level that lies close to the threshold of the incident channel. If this quasibound level is the only quasibound level in the manifold supported by the potential, then the elastic cross section also attains a large value typical of a zero-energy resonance. However, if the potential supports more than one quasibound level, then a suppression of the elastic cross section may accompany the enhancement of the inelastic cross section [18]. This is what occurs for Ar $+H_2(v=5,j=1)$. The limiting value of the elastic cross section is smaller than that of the adjacent vibrational levels as can be inferred from the values of the scattering lengths listed in Table I. Interestingly, this same anomalous behavior was seen previously [18] for Ar+$H_2(v=5,j=1)$ using a different PES.

Figure 12 shows state-to-state cross sections for Kr $+H_2(v,j=1)$ as a function of energy. The curves appear very similar to those in Fig. 11 for Ar+$H_2(v,j=1)$. The resonances, however, tend to be more randomly distributed for these higher v states compared to the case for $v=1$. For example, the $v=5$ and $v=8$ curves show no similarities in the resonance structures between the two systems. It is interesting to observe the behavior of nonresonant rovibrational energy transfer with increasing v. In going from $v=1$ to $v=5$, the trend for the $j'=5$ curve is to move downward in comparison to the $j'=3$ curve. This is consistent with the behavior of the $\Delta j=4$ and $\Delta j=2$ curves for para-H_2 as seen in Fig. 10. The trend is then reversed for higher vibrational levels. For $v>6$, the $j'=5$ curve surpasses the $j'=3$ curve and begins to approach the dominant $j'=7$ curve. This changeover is due to the decreasing energy gaps that occur with increasing v which allow the competitive balance between energy-gap and angular momentum gap behavior to be shifted.

The total quenching cross sections may be multiplied by the collision velocity to produce rate coefficients that are independent of temperature in the ultracold regime. These limiting rate coefficients are conveniently expressed in terms of the imaginary part of a complex scattering length $a_{vj}=\alpha_{vj}-i\beta_{vj}$ with $\alpha_{vj}=-\tan\delta_{vj}/k_{vj}$ and $\beta_{vj}=\sum_{v'j'}\sigma_{vj\to v'j'}k_{vj}/4\pi\hbar$, where k_{vj} is the wave vector in the

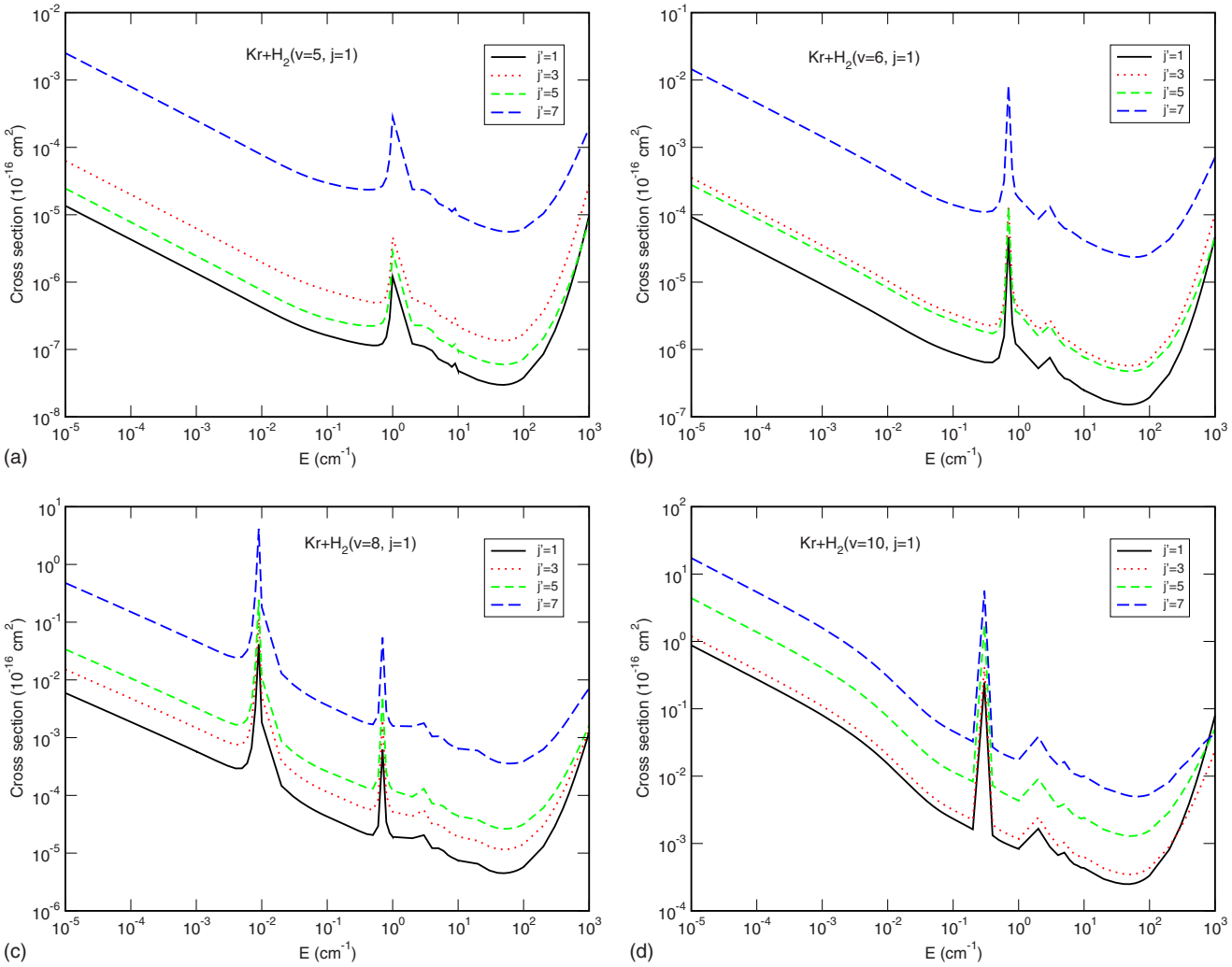

FIG. 12. (Color online) State-to-state collision cross sections for $Kr+H_2(v,j=1)$ making transitions to $H_2(v'=v-1,j')$. The curves are defined by the final rotational level shown in the legend.

incident channel. For convenience, we evaluate α_{vj} from the limiting value of the elastic cross section given by $\sigma_{vj\to vj}=4\pi(\alpha_{vj}^2+\beta_{vj}^2)$. This yields only the magnitude of the scattering length but not its sign. Table I gives scattering lengths for Ar and Kr collisions with $H_2(v,j)$. The elastic component decreases with v for $v<5$ for both systems. For $v>5$, the efficiency of elastic scattering increases for Kr and remains roughly constant for Ar. The scattering lengths for the ground state $H_2(v=0,j=0)$ are consistent with those reported previously [19,31,32].

IV. SUMMARY AND CONCLUSIONS

Previous studies of $He+H_2$ and Ar+para-H_2 collisions have been extended in this work to include Ar+ortho-H_2 and $Kr+H_2$ collisions. The competitive balance between energy-gap and angular momentum gap behavior is used to explain trends in the state-to-state cross sections. The energy dependence of the cross section for all three systems is similar in the ultracold limit to the thermal energy regime. Cross sections for the three systems exhibit minima at incident energies that are comparable to the well depth of their van der Waals interaction potentials. The absence of shape resonances in the cross sections for the He-H_2 system is attributed to its shallow van der Waals interaction potential (~ 10 cm^{-1}) and light mass. For such weakly anisotropic systems, there is no *a priori* predictable behavior in the relative magnitudes of the state-to-state cross sections. On the other hand, the results for Ar and Kr colliders are found to be qualitatively very similar. This suggests that the dynamics of H_2 collisions with heavy noble-gas atoms are relatively insensitive to details of the PES. This observation may be useful for analyzing the behavior of systems involving other rare gas atoms at low collision energies [31].

The effect of vibrational excitation on the state-to-state cross sections of orthohydrogen and parahydrogen collisions with Ar and Kr has been explored. It is found that the overall effect of vibrational excitation is to enhance the cross sections for both systems. However, at ultralow energies, the enhancement is found to be about 2 orders of magnitude greater for ortho-H_2 collisions than para-H_2 collisions. For the former, the cross section increases by about 7 orders of magnitude when the vibrational quantum number of the H_2

molecule is increased from 1 to 10. This is in contrast to the He-H_2 system for which the cross section increases by only about 4 orders of magnitude for the same range of vibrational levels [12]. The higher cross sections for the Ar and Kr systems is attributed in part to resonance enhancement and stronger dispersive forces in the interaction potential.

The cross sections presented here for Ar and Kr are largely insensitive to the details of the interaction potentials because the anisotropy in both cases is sufficiently large. It is often difficult, however, to reliably determine the strength of the anisotropy for a given system. For example, the PES of Boothroyd *et al.* [29] has significantly greater anisotropy than the PES of Muchnick and Russek [21] for the same He+H_2 system. Although the PES of Muchnick and Russek [14] is believed to be more reliable, the state-to-state cross sections computed using the PES of Boothroyd *et al.* have relative magnitudes that are qualitatively similar to those described here for Ar and Kr. For the Ar+H_2 system, the PES of Schwenke *et al.* [30] has less anisotropy than that of Bissonnette *et al.* [27] and may give qualitatively different cross sections than those reported here. It is hoped that the present study will motivate further refinements of these interaction potentials as well as experimental investigations of rotational and vibrational relaxation of molecules at cold and ultracold temperatures.

ACKNOWLEDGMENTS

This work was supported by the National Science Foundation through Grants No. PHY-0555565 (B.C.H. and N.B.) and No. PHY-0554794 (L.O. and R.C.F). We thank R. J. Le Roy for providing the potential subroutine for Kr+H_2.

[1] J. M. Doyle, B. Friedrich, J. Kim, and D. Patterson, Phys. Rev. A **52**, R2515 (1995).
[2] N. Balakrishnan, G. C. Groenenboom, R. V. Krems, and A. Dalgarno, J. Chem. Phys. **118**, 7386 (2003).
[3] R. V. Krems, H. R. Sadeghpour, A. Dalgarno, D. Zgid, J. Klos, and G. Chalasinski, Phys. Rev. A **68**, 051401(R) (2003).
[4] T. V. Tscherbul, J. Klos, L. Rajchel, and R. V. Krems, Phys. Rev. A **75**, 033416 (2007).
[5] N. Balakrishnan, A. Dalgarno, and R. C. Forrey, J. Chem. Phys. **113**, 621 (2000).
[6] P. M. Florian, M. Hoster, and R. C. Forrey, Phys. Rev. A **70**, 032709 (2004).
[7] B. Yang, H. Perera, N. Balakrishnan, R. C. Forrey, and P. C. Stancil, J. Phys. B **39**, S1229 (2006).
[8] N. Balakrishnan and A. Dalgarno, J. Chem. Phys. A **105**, 2348 (2001).
[9] K. Tilford, M. Hoster, P. M. Florian, and R. C. Forrey, Phys. Rev. A **69**, 052705 (2004).
[10] J. Doyle, B. Friedrich, R. V. Krems and F. Masnou-Seeuws, Eur. Phys. J. D **31**, 149 (2004).
[11] O. Dulieu, M. Raoult, and E. Tiemann, J. Phys. B **39** (2006) (Special Issue).
[12] N. Balakrishnan, R. C. Forrey, and A. Dalgarno, Phys. Rev. Lett. **80**, 3224 (1998).
[13] R. C. Forrey, N. Balakrishnan, A. Dalgarno, M. R. Haggerty, and E. J. Heller, Phys. Rev. Lett. **82**, 2657 (1999).
[14] T.-G. Lee, C. Rochow, R. Martin, T. K. Clark, R. C. Forrey, N. Balakrishnan, P. C. Stancil, D. R. Schultz, A. Dalgarno, and G. J. Ferland, J. Chem. Phys. **122**, 024307 (2005).
[15] A. Mack, T. K. Clark, R. C. Forrey, N. Balakrishnan, T.-G. Lee, and P. C. Stancil, Phys. Rev. A **74**, 052718 (2006).
[16] R. C. Forrey, Phys. Rev. A **63**, 051403(R) (2001).
[17] R. C. Forrey, Phys. Rev. A **66**, 023411 (2002).
[18] J. C. Flasher and R. C. Forrey, Phys. Rev. A **65**, 032710 (2002).
[19] N. Uudus, S. Magaki, and N. Balakrishnan, J. Chem. Phys. **122**, 024304 (2005).
[20] H. Wei, R. J. Le Roy, R. Wheatley, and W. J. Meath, J. Chem. Phys. **122**, 084321 (2005).
[21] P. Muchnick and A. Russek, J. Chem. Phys. **100**, 4336 (1994).
[22] M. M. Audibert, Doctorate thesis, Universit de Paris-Sud, 1976; M. M. Audibert, C. Joffrin, and J. Ducuing, J. Chem. Phys. **61**, 4357 (1974); M. M. Audibert, R. Vilaseca, J. Lukasik, and J. Ducuing, Chem. Phys. Lett. **31**, 232 (1975).
[23] A. Kalinin, O. Kornilov, L. Y. Rusin, and J. P. Toennies, J. Chem. Phys. **121**, 625 (2004).
[24] F. A. Gianturco, T. Gonzolez-Lezana, G. Delgado-Barrio, and P. Villareal, J. Chem. Phys. **122**, 084308 (2005).
[25] Y. Xiao and B. Poirier, J. Phys. Chem. A **110**, 5475 (2006).
[26] Y. Li and C. D. Lin, J. Phys. B **32**, 4877 (1999).
[27] C. Bissonnette, C. E. Chauqui, K. G. Crowell, and R. J. Le Roy, J. Chem. Phys. **105**, 2639 (1996).
[28] J. M. Hutson and S. Green, MOLSCAT computer code, version 14 (1994), distributed by Collaborative Computational Project No.6 of the Engineering and Physical Sciences Research Council (UK).
[29] A. I. Boothroyd, P. G. Martin, and M. R. Petersen, J. Chem. Phys. **119**, 3187 (2003).
[30] D. W. Schwenke, S. P. Walch, and P. R. Taylor, J. Chem. Phys. **98**, 4738 (1993).
[31] P. Barletta, J. Tennyson, and P. F. Barker, Phys. Rev. A **78**, 052707 (2008).
[32] P. Barletta, Eur. Phys. J. D **53**, 33 (2009).